EFFECT OF THE ADDITIVE MANUFACTURING PROCESS ON CUTTING FORCES IN HYBRID MANUFACTURING

Michael Gomez[1], Andrew Honeycutt[1], Jarred Heigel[2], and Tony L. Schmitz[1]
[1]Department of Mechanical Engineering and Engineering Science
University of North Carolina at Charlotte, Charlotte, NC
[2]Production Systems Group
National Institute of Standards and Technology*, Gaithersburg, MD

INTRODUCTION

Powder bed fusion (PBF) enables metal components with complex geometries to be made via additive manufacturing (AM). Disadvantages of AM are rougher surface finish and lower achievable dimensional tolerances compared to computer numerically-controlled (CNC) machining [1]. Hybrid manufacturing combines additive and subtractive manufacturing strategies, which allows complex metal parts to be produced with the required surface finish and accuracy. An important consideration in hybrid manufacturing is the effect of the additive step on material removal in the subtractive step. Specifically, the cutting force is typically described using a force model that includes empirical coefficients that relate the required force to the commanded chip width and thickness. This paper explores the effects of the PBF process, as well as follow-on heat treating, on workpiece surface and material characteristics and, therefore, the corresponding cutting force coefficients.

CUTTING FORCE MODEL

The cutting force, which is often described using a mechanistic model with empirical coefficients, directly influences both the allowable, chatter-free material removal rate and surface location error (i.e., the geometric error caused by forced vibration during stable cutting). Surface location error is the difference between the locations for the actual and commanded surfaces. Therefore, an accurate cutting force model is needed to predict process parameters that will produce high quality parts.

The cutting force model applied in this study relates the uncut chip dimensions to the cutting force components using Eqs. 1-3:

$$F_t = k_t b h + k_{te} b \quad (1)$$

$$F_r = k_r b h + k_{re} b \quad (2)$$

$$F_a = k_a b h + k_{ae} b \quad (3)$$

where F_t, F_r, and F_a are the tangential, radial, and axial direction force components, respectively, which rotate with the cutter. The k_t, k_r, and k_a coefficients relate the force to chip area, where b is the axial depth of cut (chip width) and h is the instantaneous chip thickness. The edge coefficients, k_{te}, k_{re}, and k_{ae}, relate the force to the axial depth only and are associated with rubbing and non-cutting contact [2].

Experiments were completed to determine the cutting force coefficients at five different feed-per-tooth values. A new cutting insert was used for each cutting test in order to minimize the effects of tool wear on the force measurements. A single tooth cutter was used in order to eliminate the effects of tooth-to-tooth runout.

WORKPIECE DESCRIPTION

A pair of workpieces are shown in Figure 1A. Each workpiece consists of a wrought 17-4 stainless steel substrate (25 mm tall, 50 mm wide, 150 mm long) and a PBF deposited feature (25 mm tall, 15 mm wide, 140 mm long). A photograph of the PBF process during the creation of these figures is provided in Figure 1B. The process is repeated twice to create two pairs of workpieces, one that is heat treated at 650 °C for 1 hr to relieve the residual stress that is inherently created during the process, and the other pair that will be tested in the as-produced condition.

Within each workpiece, there are three material conditions of interest: the wrought substrate, the AM surface material, and the AM bulk material. The wrought substrate is a traditionally produced material that provides a baseline for which to compare the AM material. The AM surface material is the portion of PBF deposited material within 1 mm of the vertical faces of PBF feature. This material incorporates both the high residual stress and the rough surface generated by the PBF process. The AM bulk material is the remainder of the PBF feature and does not include the rough PBF surfaces.

Six different force models were established for the as-produced (not heat treated) substrate, AM surface, and AM bulk materials, as well as the heat-treated substrate, AM surface, and AM bulk materials. There were two goals for this approach. First, the impact of

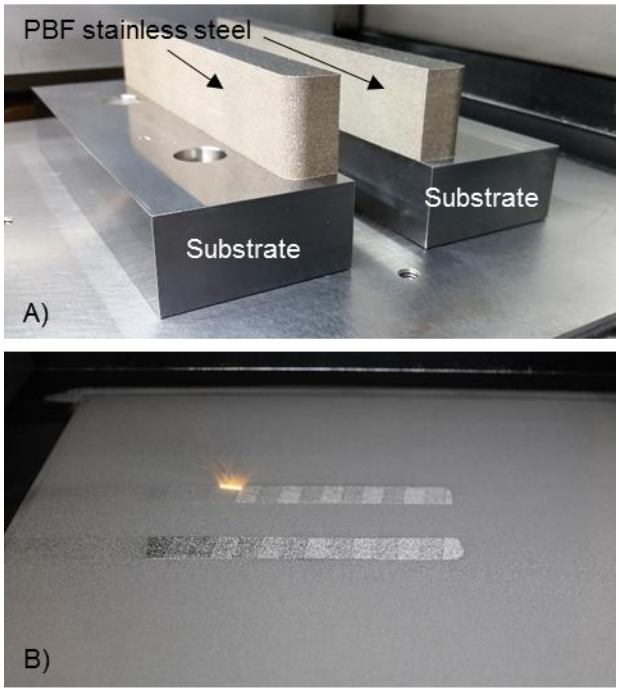

Figure 1. A) One pair of workpieces mounted on the PBF build platform. Each workpiece has a PBF stainless steel feature (top section) deposited on a wrought stainless steel substrate (bottom section with holes). B) Photograph of the PBF build process during the deposition of 1 pair of workpieces.

a variety of AM processing and post-processing effects can be compared to a baseline, as shown in Table 1. The as-produced AM surface of workpieces 1 and 3 has the greatest number of effects from the AM processing, including the residual stress and rough surface generated by the process, and any other possible differences between wrought and AM 17-4 stainless steel. The number of effects decreases by investigating the AM bulk, which removes the effect of the rough surface, and heat treating to remove residual stress. The second goal, is to demonstrate the difference between post-process machining that is required on many AM parts, which are likely heat treated prior to machining, and the intermittent machining that is implemented during hybrid processes, in which heat treatment is not performed before machining.

NON-LINEAR OPTIMIZATION MODEL

Tool wear can significantly affect cutting forces and machining stainless steel can lead to non-negligible wear rates. Therefore, a nonlinear optimization algorithm was used to determine the cutting force coefficients for each of the three materials within a single workpiece (wrought, AM surface, and AM bulk)

Table 1. Overview of the created workpieces and material regions of interest.

Workpiece	Material region	Heat treat	Effects
1 & 3	Substrate	no	- As-received baseline
1 & 3	AM surface	no	- Rough PBF surface - Residual stress - AM material difference from wrought
1 & 3	AM bulk	no	- Residual stress - AM material difference from wrought
2 & 4	Substrate	yes	- Heat-treat baseline
2 & 4	AM surface	yes	- Rough PBF surface - AM material difference from wrought
2 & 4	AM bulk	yes	- AM material difference from wrought

[3]. Using the experimental cutting force coefficients, a comparison can be made between the as-produced and annealed PBF cases. The nonlinear optimization method is advantageous because only a single cutting trial is required to determine the cutting force coefficients in a least-squares best fit sense.

The least-squares, nonlinear optimization method simulates the cutting forces over one cutter revolution using Equations 1-3. It then compares the simulated cutting forces to the measured cutting forces over a range of reasonable values for each of the six cutting force coefficients. The nonlinear optimization method seeks to minimize the difference between the simulated cutting forces and the measured cutting forces by Equation 4, where the fixed direction x, y, and z force components are determined from a projection of the rotating force components from Equations 1-3 using the cutter angle.

$$f(k_t, k_r, k_a, k_{te}, k_{re}, k_{ae}) = \sum \left\| \begin{Bmatrix} F_x \\ F_y \\ F_z \end{Bmatrix}_{simulated} - \begin{Bmatrix} F_x \\ F_y \\ F_z \end{Bmatrix}_{measured} \right\|^2 \quad (4)$$

CUTTING FORCE COEFFICIENTS

The machining setup for cutting force measurements is shown in Figure 2. The milling process was carried out using a new cutting insert (Sandvik Coromant

390R-070204E-MM S30T)† for each test to reduce the effects of tool wear on the force measurements.

A radial runout measurement was performed for the first set of cutting inserts. The purpose of these tests was to determine the change in cutting diameter as the insert is replaced. The normalized results are shown in Table *2*, where the measurements are performed using the machine spindle, a Mitutoyo dial indicator, and a Noga dial gage holder.

Figure 3 shows the results for the tangential and radial cutting force coefficients, k_t and k_r, at the commanded feed per tooth values as generated by the non-linear optimization model. Although there is some difference between the three materials at different feed per tooth values, there is generally no significant difference between the results for each material on the two as-produced workpieces. The results shown in Figure 3 demonstrate the repeatability in measurement results from the machining tests of as-produced workpieces.

Repeatability tests were conducted for the annealed workpieces 2 and 4. The results of the

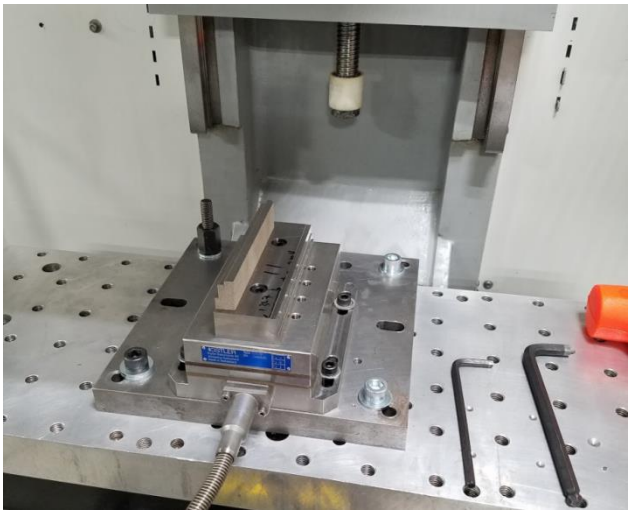

Figure 2. Machining experiment setup. The workpieces were mounted on a Kistler 9257B three-axis force dynamometer. All machining experiments were performed on a Haas TM-1 CNC milling machine.

Table 2. Radial measurement runout results.

Insert	Runout (µm)
1	0
2	152
3	50.8
4	25.4
5	76.2
6	127
7	0
8	25.4
9	-25.4
10	102

† Certain commercial equipment, instruments, or materials are identified in this paper in order to specify the experimental procedure adequately. Such identification is not intended to imply recommendation or endorsement by the National Institute of Standards and Technology, nor is it intended to imply that the materials or equipment identified are necessarily the best available for the purpose.

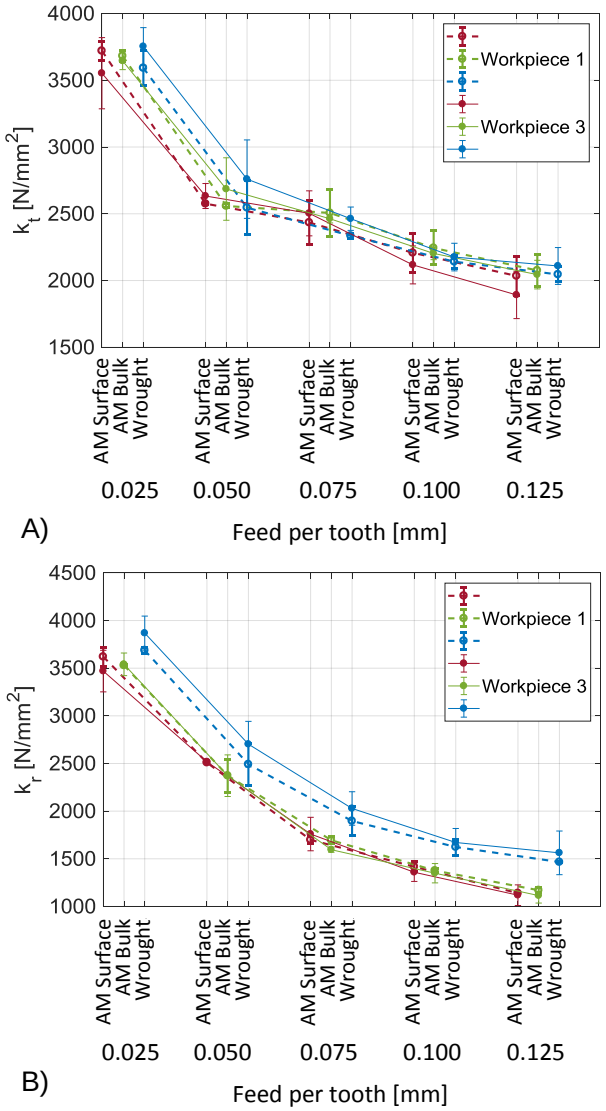

Figure 3. Mean values and 95% confidence intervals for A) tangential cutting force coefficients and B) radial cutting force coefficients for the as-produced workpieces. There were two sets of tests carried out on workpiece 1 and three sets of tests carried out on workpiece 3.

tangential cutting force coefficients and radial cutting force coefficients are provided in Figure 4. There is again no appreciable difference between the tangential cutting force coefficients for the two workpieces. Regarding the radial cutting force coefficients, while the error bars do not overlap between the two workpieces in each instance, it can be seen that there is limited variation in radial cutting force coefficients between the two.

The cutting force coefficient results for both the tangential and radial components can be grouped together to form a total of six cutting models for the as-produced and annealed workpiece categories. The results are shown in Figure 5. The annealing process increases both the tangential and radial cutting force coefficients (comparing solid line of the annealed cases to the dashed lines of the as-produced cases). A marked difference is apparent in the AM bulk material, where annealing increases both tangential and radial cutting force coefficients by a statistically significant amount.

From Figure 3 through Figure 5, it can be observed that the both the tangential and radial cutting force coefficients reduce with increasing feed

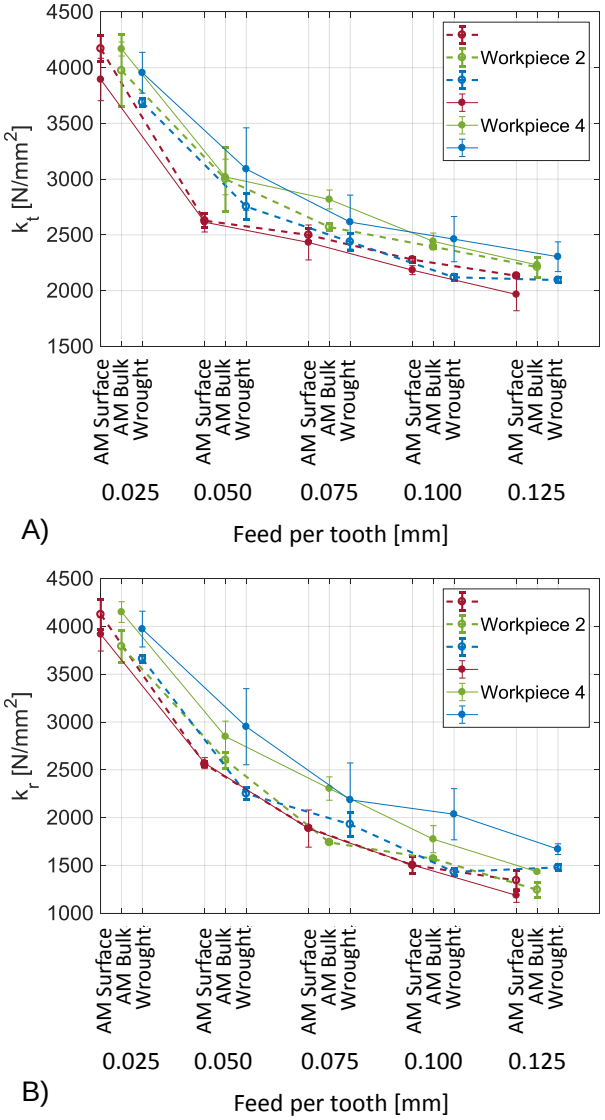

Figure 4. Mean values and 95% confidence intervals for A) tangential cutting force coefficients and B) radial cutting force coefficients for the annealed workpieces. There were two sets of tests carried out on workpiece 2 and three sets of tests carried out on workpiece 4.

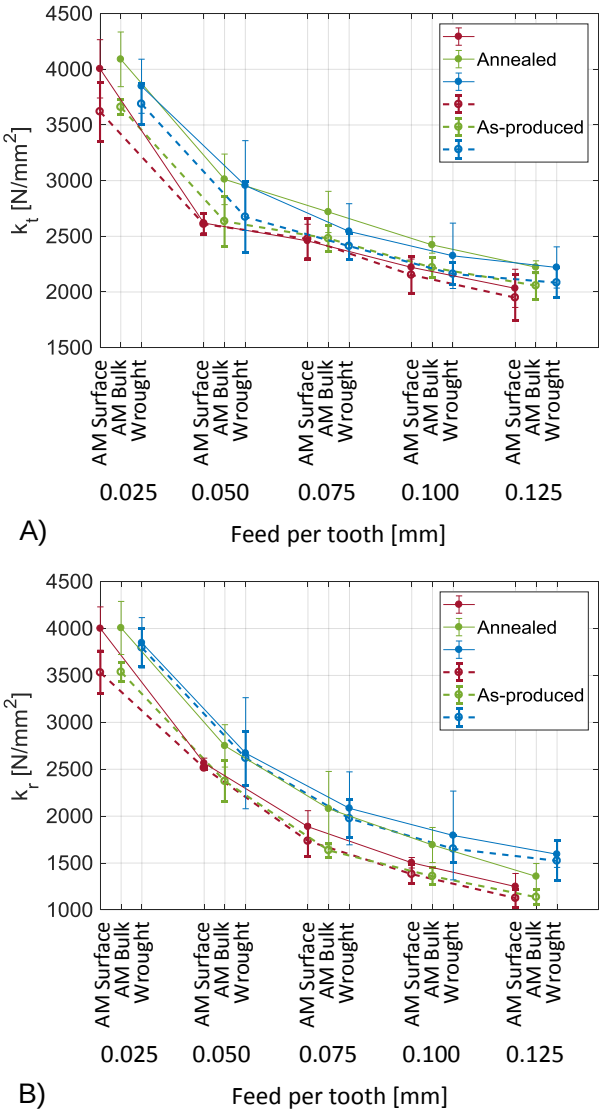

Figure 5. Comparison of the A) tangential cutting force coefficient and the B) radial cutting force coefficient for the as-produced and annealed workpieces materials.

per tooth. This phenomena occurs when the chip thickness approaches the cutting edge radius [4]. In this case, the rake angle appears to be negative which changes the chip formation [5]. To verify this behavior, a cutting insert was sectioned using wire electrical discharge machining (EDM) to expose the cutting edge radius. The cutting insert was placed in an scanning electron microscope (SEM) to obtain the approximate cutting radius. It was determined that the cutting edge radius is approximately 49 µm; see Figure 6. Therefore, a different cutting force model is needed to capture this effect. In follow-on analyses, the Kienzle force model will be applied [6]:

$$F_t = K_t b h^{1-m_t} \quad (5)$$

$$F_r = K_r b h^{1-m_r} \quad (6)$$

$$F_a = K_a b h^{1-m_a} \quad (7)$$

where there is a power law dependence on the chip thickness through the m coefficients and new cutting force coefficients, K, are defined.

ELASTIC MODULUS

A non-destructive means for identifying the elastic modulus was implemented. Specimens were machined from the initial workpiece and impulse excitation was used to determine the natural frequencies [4]. In these experiments, each specimen was subjected to a short duration impact from a dropped 9.5 mm diameter sphere; the response was measured using a digital microphone and the natural frequencies, f_n, were observed in the frequency domain. Free-free boundary conditions were approximated by placing the specimens on a soft foam base, as shown in Figure 7.

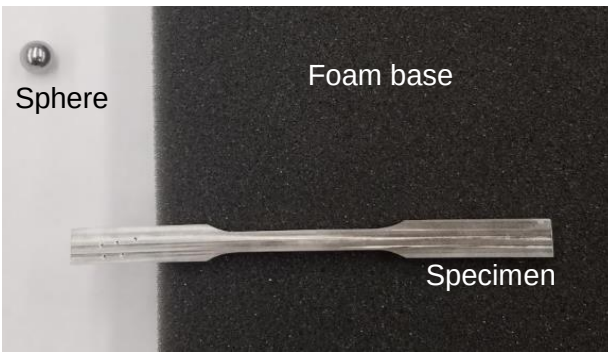

Figure 7. Experimental setup for the impulse excitation testing. The specimens were placed on a foam support and subjected to an impact from a dropped sphere. The sound was recorded using a microphone.

Once the natural frequencies were known, a finite element (FE) model was completed for the specimen and the elastic modulus was adjusted until the natural frequencies matched. There were two AM specimens used for the FE analysis: 1) as-produced; and 2) annealed. The specimens created using the wrought material will be measured in follow-on work. The measured dimensions were used to model the specimens in PTC Creo Parametric 3.0 and Creo Simulate was used to perform FE analysis. The measured density, ρ, and assumed Poisson's ratio, ν, were assigned to the material which was subject to a free-free boundary condition. The simulation produced the first six vibrational modes. The elastic modulus was used as a fitting parameter for a best fit to the first three natural frequencies; see Figure 8.

Table 3 shows the first three measured natural frequencies for both AM specimens, as well as the measured Poisson's ratio and density and the assumed modulus of elasticity that brings the

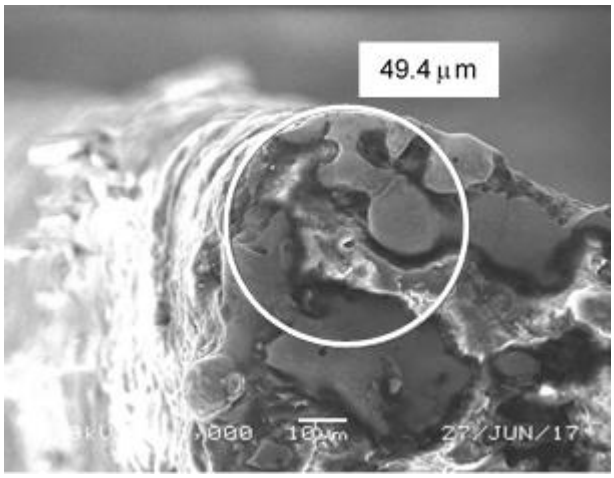

Figure 6. SEM image of the cutting edge radius.

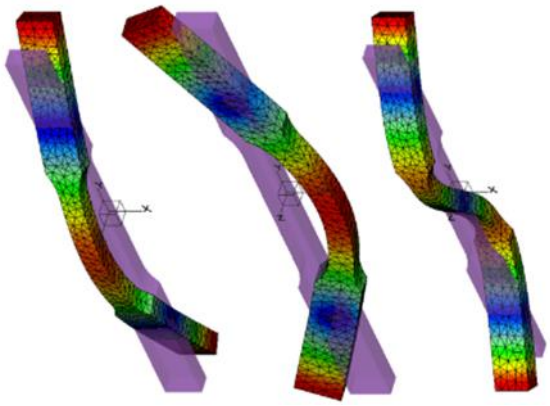

Figure 8. The first (left), second (middle), and third (right) bending modes produced by the FE simulation

Table 3. Material properties for the AM specimens.

Properties	As-produced	Annealed
f_{n1} (Hz)	1352	1378
f_{n2} (Hz)	1642	1667
f_{n3} (Hz)	3984	4058
υ	0.29	0.29
ρ (kg/m^3)	7873	7918
E (GPa)	188	195

simulation into agreement with the measurements. It is observed that both the density and elastic modulus were higher from the annealed specimens.

HARDNESS

Hardness tests were conducted on a Wilson Rockwell Series 2000 testing machine. A Rockwell C hardness scale, HRC, was selected. The results of the hardness tests are shown in Figure 9. The horizontal band represents the typical HRC values for 17-4 stainless steel. It can be seen that annealing reduced the hardness in the wrought material. However, it increased the hardness for the AM material. There is a characteristic increase in HRC values in both the in-plane (top) and out-of-plane (side) build direction.

CONCLUSIONS

The purpose of this study was to assess variations in the cutting force model for wrought and additively manufactured workpieces. Two conditions were considered: as-produced and annealed. The force model is critical because it is used in analyses used to predict machining stability and surface location errors. Therefore, an improved understanding of the effects of the additive manufacturing process on cutting force coefficients will give new insight into hybrid manufacturing strategies.

The results showed only minor differences in the coefficients between the various material states. The strongest effect was annealing, which increased the coefficients in all cases, particularly for the bulk additively manufactured material. A general trend of decreasing coefficients with increasing feed was observed. This is due to a change in the apparent rake angle and is well-known. To address this effect, the linear force model will be updated using the Kienzle model [6].

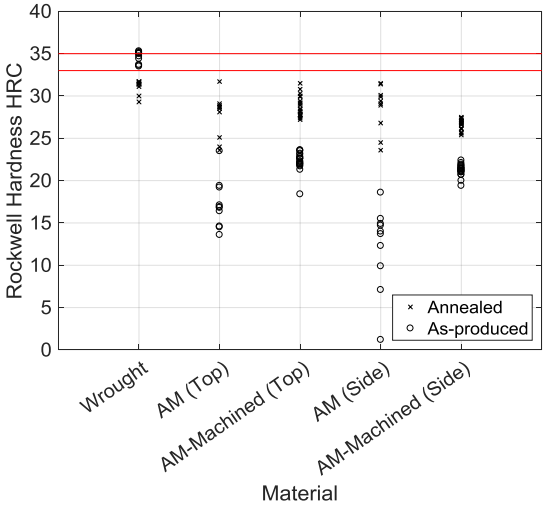

Figure 9. Rockwell hardness values for the wrought, as-produced, and annealed specimens. There were ten measurements completed for each case.

ACKNOWLEDGEMENTS

The authors gratefully acknowledge partial financial support from the UNC Charlotte Center for Precision Metrology Affiliates Program.

REFERENCES

[1] Cooke, A.L. and Soons, J.A., 2010, Variability in the geometric accuracy of additively manufactured test parts, 21st Annual International Solid Freeform Fabrication Symposium, Austin, TX

[2] Schmitz, T. and Smith, K.S., 2008, Machining Dynamics: Frequency Response to Improved Productivity, Springer, New York, NY.

[3] Rubeo, M. and Schmitz, T., 2016, Mechanistic force model coefficients: A comparison of linear regression and nonlinear optimization, Precision Engineering, 45: 311-321.

[4] Cossolino, L.C. and Pereira, A.H.A, 2010, Elastic moduli: Overview and characterization methods, ATCP Physical Engineering, Technical Review ITC-ME/ATCP, 10-11.

[5] Coelho, R.T., Braghini Jr., A., Valente, C.M.O. and Medalha, G.C., 2003, Experimental evaluation of cutting force parameters applying mechanistic model in orthogonal milling, Brazilian Society of Mechanical Science & Engineering, 247-248.

[6] Kienzle, O., 1952, Die Bestimmung von Kräften und Leistungen an spanenden Werkzeugen und Werkzeugmaschinen, In: Zeitschrift des Vereins deutscher Ingenieure, 657-662.